The Role of Endwall Shape Optimization in the Design of Supersonic Turbines for Rotating Detonation Engines

Noraiz Mushtaq
Laboratory of Fluid Machines (LFM)
Department of Energy - Politecnico di Milano
Via Lambruschini 4, 20156 Milan, Italy
Email: noraiz.mushtaq@polimi.it

Giacomo Persico
Laboratory of Fluid Machines (LFM)
Energy Department - Politecnico di Milano
20156 Milan, Italy
Email: giacomo.persico@polimi.it

Paolo Gaetani*
Laboratory of Fluid Machines (LFM)
Energy Department - Politecnico di Milano
20156 Milan, Italy
Email: paolo.gaetani@polimi.it

ABSTRACT

Rotating detonation engines (RDE) are characterized by a thermodynamic cycle with an efficiency gain up to 15% at medium pressure ratios with respect to systems based on the conventional Joule-Bryton cycle. Multiple turbine designs can be considered and this paper deals with the supersonic inlet configuration. After having reviewed the main design steps of an exemplary RDE supersonic turbine, the paper focuses on the considerable effects that endwall losses have on the performance of supersonic-inlet turbines and on the reasons why endwall contouring is strongly recommended for an efficient design. Parametric analyses, carried out by a novel in-house mean-line code validated against CFD, reveal that endwall friction losses contribute significantly to the overall stage loss. Endwall boundary layers also reduce the effective area, which can be critical for the self-starting capability of the supersonic channel. Therefore, a variable blade height geometry

*Corresponding author.
TURBO-22-1161, Gaetani P.

is necessary to extend the design space and guarantee a higher efficiency with respect to a constant-span configuration. The in-house CFD-based evolutionary shape optimization code was adapted to search for the optimal endwall shape for these unconventional machines. The optimal shape reduces shock losses and deviation angles and provides a significant gain in efficiency and work extraction. Finally, a novel technique is proposed to design the three-dimensional shape of the rotor based on the method of characteristics and tailored on the flow delivered by the stator.

Keywords: Rotating Detonation Engine (RDE); supersonic turbines; endwall losses; shape optimization

1 INTRODUCTION

In the effort of reducing the impact of human activities on the environment and mitigating the effects of climate change, ever more efficient energy conversion systems are required. In an energy scenario dominated by the combination of multiple technologies exploiting diverse energy sources, gas turbines will play a critical role in balancing the discontinuous supply by non-schedulable renewable energy sources, providing an important prerequisite for a massive introduction of renewable technologies in the overall energy mix.

In this context, conventional gas turbines have to be improved by means of new architectures, new fuels and new working principles. As for the fuels, hydrogen-based compounds like pure H_2, NH_3 and Sustainable Aviation Fuels (SAFs) can replace the carbon-based compounds like JetA and CH_4 [1, 2]. Moreover, H_2 has the undeniable advantage of a fast combustion that allows to reduce the engine weight and possibly the transient in regulation. When considering alternative cycle configurations, an opportunity to improve the gas turbine efficiency is to switch from deflagrative combustion to detonating combustion, which is expected to be more efficient thanks to the pressure gain in the combustion process. Among the possible detonating combustion devices, the rotating detonation engines (RDEs) appear to be the most promising due to the expected increase in the efficiency and to the simplicity of its design and assembly without the requirement of mechanical actuations.

From the theoretical point of view, a RDE should allow for a decrease in fuel consumption compared to traditional gas-turbine engines [3, 4], an increase in total pressure thanks to detonation (up to 15%) [5] which allows to reduce the number of compressor stages for a given overall pressure ratio, an increase of gas turbine thermal efficiency [6, 7] and plant efficiency up to 14% over a conventional turbine [8] for intermediate pressure ratios. To translate this appealing concept into an engineering technology, the RDE development process has to face multiple challenges, and a crucial one is the complex behaviour of the detonation combustion and of the supersonic flow entering into the turbine. In the last 5 years several successful experimental investigations have supported such theoretical expectations, paving the way for enhancing the entrance into service of such technology [9–15]. Some comprehensive reviews on the combustion issues can be found in [16, 17].

Another critical issue is the design of efficient turbines and transition ducts connecting the combustion chamber to the first turbine stage. On this topic substantial contributions can be found in [18–22], which report a preliminary studies and advanced aerodynamic investigations focused on the turbine, and in [23, 24] focused on combustion-turbine coupling. In this context, both a supersonic and a subsonic first turbine stage can be considered, having each of them pros and cons. The supersonic inlet stage allows for a huge work extraction, that lowers the gas temperature rather quickly, at the expense of an efficiency reduction with respect to more conventional subsonic inlet designs. The selection of the turbine configuration also impacts on the design of the transition duct connecting the machine with the pulsating combustion chamber [24]. In case of supersonic inlet stage, the efficiency is the most critical parameter that demands for the application of state-of the-art and rigorous design techniques to prevent an excessive penalty. The primary source of losses in such turbines are the shock waves originated upstream of the stator leading edge, the shock reflections within the cascades, the profile losses, the wake mixing and the endwall boundary layer.

In [22, 25] the fully 3D design of a supersonic turbine stage is addressed by the combination of mean-line codes and the method of characteristic for the blade design, complemented by computational fluid dynamics (CFD) for the detailed analysis of the designed stage. Endwall op-

timization for subsonic turbines was carried out in [26], but endwall losses and their effects were not quantified or discussed. For supersonic inlet turbines, no prior knowledge can be found about the relative weight of endwall losses, the impact of endwall boundary layer on the starting limit and the benefits of endwall shape optimization. In fact, in actual turbines, the stators and rotor are transonic with a small extension of the supersonic region; only some steam turbine applications foresee supersonic inlet for rotors [27]. In the open literature some correlations are proposed for the endwalls loss evaluation [28–30] and all of them foresee a non-negligible impact on the efficiency due to the high flow speed. For the RDE application, the expected impact of endwall losses seems to be even higher than those normally found for conventional transonic turbines, for that only the rear part of the cascade experiences high Mach number flows. Moreover, at high Mach number the boundary layer development introduces an additional issue related to the blockage that considerably modifies the whole cascade flow field and thus the operation.

This relevant design aspect is believed to demand a dedicated study; the present paper aims at providing a quantitative insight in the effect of endwall loss in supersonic turbines and demonstrates the beneficial effects of endwall optimisation by applying advanced and systematic methodologies, such as the one applied in [31]. The paper first describes the methodologies applied in the present research, then it focuses on the 3D stage design with both simplified and optimal endwalls, and it finally derives some relevant conclusions on the benefits of the endwall optimisation in supersonic turbines.

2 METHODS

The present study was performed by combining CFD simulations, a mean-line code featuring a characteristic-based profile design, and an evolutionary shape optimization procedure. Therefore, a brief description of the in-house developed tools and a clear definition of the accuracy and modelling of the CFD simulations will be presented in the next paragraphs.

2.1 Computational flow model

3D steady-state simulations were carried out applying the Ansys CFX solver, which implements a pressure-based implicit coupled solver with co-located grid arrangement. The advection

terms in both the flow and turbulence equations were modelled by a high-resolution scheme implemented as a Total Variation Diminishing (TVD) algorithm, which has demonstrated to be accurate in modelling shock wave reflections [32]. Turbulence closure was achieved through the $k-\omega$ SST model and y^+ was kept below 1 on all the wall surfaces to obtain a correct boundary layer resolution. The working fluid is air which is assumed to be a perfect gas.

Pressure, temperature and velocity are all assigned at inlet because the flow is supersonic. The blade, the hub and the shroud are modelled as adiabatic and no-slip walls. The lateral boundaries are periodic and a mixing-plane interface was employed in the stator-rotor coupled simulations. Computations were considered at convergence when all the residuals were below $5 \cdot 10^{-6}$.

Solver ability to accurately simulate a problem with shocks and expansion waves was assessed against two test cases: the Sod shock tube [33] and the 2D compression corner [34–36]. In the first problem the solver must be able to properly follow a shock wave, a contact surface and an expansion wave that are moving in different direction and at different speed, while the second one replicates the shock/boundary layer interaction problem, which incorporates altogether the difficulties of turbulence, compressibility, and viscous-inviscid interaction phenomena. A thorough description of the test cases and of the CFD set-up for the solver validation is reported in [25].

The mesh independence analysis was performed using the grid convergence method [37]: for both the stator and the rotor, structured meshes composed by 4.5 million, 9 million and 18 million hexahedral cells were tested. The reference quantity selected for the independence analysis is the entropy rise: notice that throughout this work the entropy was always calculated considering the mixed-out flow calculated by the procedure presented in [38]. This choice was made after observing that a mass flow average on a local section underpredicts optimistically the losses, since it underestimates all the mixing process and the associated entropy production that takes place downstream of that section. The 9 million cells mesh (200k cells per layer with 45 layers in radial direction) satisfied the independence condition, with a grid convergence index from the fine to the medium mesh of 0.21% for the stator and 0.70% for the rotor. In addition, the grid convergence index for power and η_{tt} are respectively 0.22% and 0.14%.

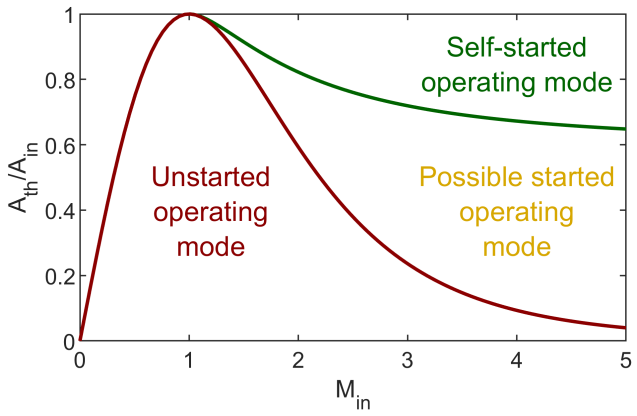

Fig. 1: CONTRACTION RATIO FOR A STARTED OR UNSTARTED BLADE ROW AT VARYING INLET MACH NUMBER.

2.2 Mean-line code

An in-house mean-line code was specifically developed for the design of a supersonic inlet turbine for RDEs. It is based on standard turbine theory and then specific features of supersonic blades are included. Here a general outline of the code capabilities is given with focus on the elements developed within this work, while a complete description with an extensive validation effort can be found in [25].

When considering supersonic turbines, the so-called self-starting of the supersonic channel, where "started" refers to an oblique shock configuration at the cascade inlet which is less dissipative than the normal shock of the "unstarted" condition, has to be verified through the Kantrowitz and Donaldson theory [39]; this is a necessary pre-requisite for an efficient operating condition of the turbine, but it has considerable effects on the design, as it limits the maximum allowable flow turning (Fig. 1 and Eq. 1). The other restriction to the design is that the axial Mach number should exceed 1 to avoid the unique incidence problem [40]. The combinations of the above conditions lead to the definition of the flow angle across the cascades.

$$\frac{A_o}{A_{in}} = \frac{g_o H_o cos(\alpha_o)}{g_{in} H_{in} cos(\alpha_{in})} > \frac{A_{th}}{A_{in}}\Big|_{self-started\ limit} \tag{1}$$

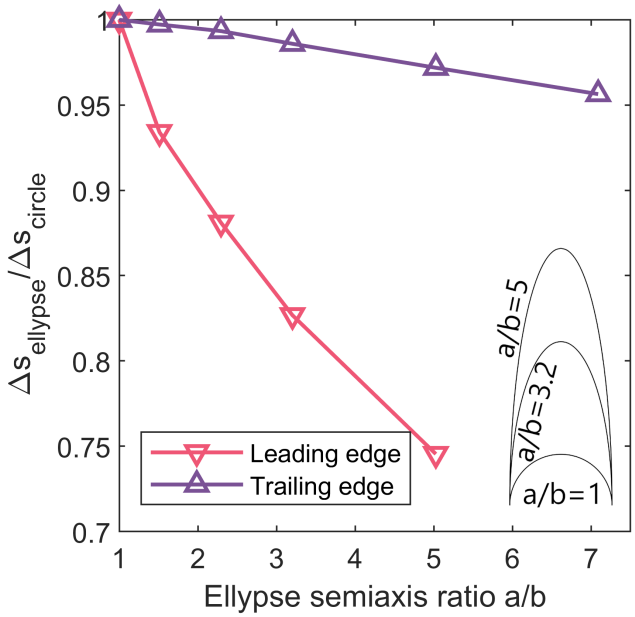

Fig. 2: ENTROPY GENERATED BY THE SUPERSONIC PROFILE WHEN THE LEADING EDGE AND THE TRAILING EDGE ARE CLOSED BY ELLIPSES OF VARIABLE SEMIAXIS RATIO.

The supersonic profile is generated by the ”vortex-flow” method, which is a specific method of characteristics developed by Goldman [41]. Once the dimensionless profile is generated and the dimensionless ratios (solidity and pitch over leading edge thickness) have been carefully selected, the dimensional blade is obtained only by assigning a proper value to the chord. Since the MOC profile has zero thickness at leading and trailing edge, the upper and lower curves are shifted of the thickness value and then closed by ellipses. Figure 2 shows a parametric analysis performed through blade-to-blade CFD simulations to select the ellipse semiaxis ratio. Increasing the leading-edge ellipse semiaxis ratio reduces the entropy jump because the effective thickness seen by the bow shock wave and the subsonic flow region behind the shock are both reduced; meanwhile by increasing the trailing-edge ellipse semiaxis ratio, mixing losses are reduced because the wake size behind the blade profile is smaller. A semiaxis ratio of 3.2 was selected for the leading edge considering also thermal and mechanical integrity, while a higher value of 5 was adopted for the trailing edge.

Finally, an accurate evaluation of the aerodynamic losses was achieved by taking into account: 1) the leading edge bow shock wave, predicted through the method developed by Moeckel for two

dimensional axial symmetric bodies [42]; 2) the first oblique shock wave reflection determined by applying the classical theory of aerodynamics [43]; 3) boundary and mixing losses obtained by first calculating the compressible turbulent boundary layer quantities using Stratford and Beavers procedure [44] and then the overall loss coefficient is evaluated by extending Stewart's method for supersonic axial Mach numbers [45]; 4) endwall losses.

This final source of entropy generation was overlooked by previous works on supersonic turbines, but, as discussed in detail in section 3.1, endwall losses have a non-negligible impact on this type of machines; thus a new methodology was implemented within this work to evaluate it. Endwall losses can be divided in two distinct contributions: dissipation in the endwall surface boundary layer and dissipation induced by secondary flows and their interaction [30]. Secondary phenomena in supersonic turbines are weak because the flow turning is significantly limited by the starting condition. In accordance with this consideration, which was also confirmed by CFD simulations, the endwall losses generated by secondary phenomena were neglected. In contrast, the dissipation on the hub and shroud surfaces is strong because the velocities are extremely high; hence, this term was calculated employing Eq. 2 proposed by Coull [30], which can be considered an evolution of the one proposed by Denton [46].

$$\xi_{ew} = 2C_D\left(\frac{A_{ew}}{Hgcos\alpha_o}\right)\int\left(\frac{T_o}{T}\right)\left(\frac{\rho}{\rho_o}\right)\left(\frac{v}{v_o}\right)^3 d\left(\frac{A}{A_{ew}}\right) \tag{2}$$

To solve the integral it is necessary to discretize the domain and determine the variables in each cell. The inlet and outlet Mach number are known from the mean-line code iterative procedure, while the Mach number on the pressure and suction side are known from the MOC; starting from this information, the data for all the other points are obtained by linear interpolation as displayed by the Mach contours of Fig. 3. Notice that for a correct comparison with the CFD simulations, the wetted surface is not composed only by the blade channel, but also by the inlet domain, interstage gap and outlet domain. After carefully examining the different options available in literature, the dissipation coefficient C_D was calculated through the correlation by Truckenbodt [47] valid for

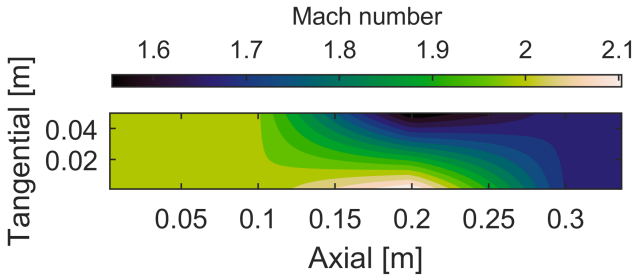

Fig. 3: MACH CONTOURS OF THE LINEARLY INTERPOLATED STATOR BLADE-TO-BLADE CHANNEL.

turbulent boundary layers (Eq. 3).

$$C_D = 2 \cdot 0.0592 \cdot 10^{-2} \cdot Re_\theta^{-\frac{1}{6}} \tag{3}$$

The validation procedure of the latest version of the code is achieved by comparing the outputs to the quantities extracted from a CFD simulation. The total-to-total efficiency and stator and rotor entropy rises predicted by the mean line code are respectively 67.73%, 61.18 J/(kg K) and 29.24 J/(kg K), while the values obtained from the CFD are 66.69%, 61.88 J/(kg K) and 34.40 J/(kg K). The lower agreement achieved for the rotor is explained by the Mach phenomenon originated from the intersection of rotor bow-shock waves, which was not considered by the mean-line code (Fig. 4). Overall, these results prove the excellent ability of the mean-line code in assessing the performance of a supersonic turbine, which makes the present code a fundamental tool in the preliminary design.

2.3 Optimization method

The optimizations documented in this study were performed applying the in-house shape optimization tool FORMA (Fluiddynamic OptimizeR for turboMachinery Aerofoils), which optimizes the shape of turbomachinery blade channels by resorting to surrogate evolutionary strategies. Multiple formulations are available, including constrained, multipoint and multiobjective optimization. FORMA combines a Bspline representation of the blade profiles and of the endwalls, the CFD model previously presented, a Kriging formulation as surrogate, and genetic algorithms. The latin

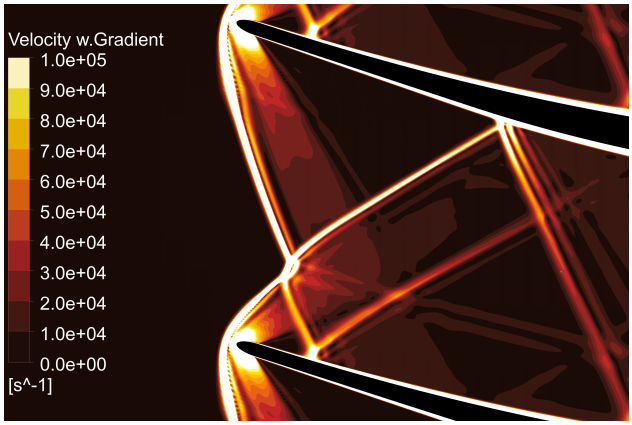

Fig. 4: MACH PHENOMENON GENERATED BY THE INTERSECTION OF ROTOR BOW-SHOCK WAVES.

hypercube sampling technique was employed to initialize the surrogate model and the number of samples selected are 10 times the number of adjustable control points. The optimization method is the constrained single-objective genetic algorithm from the JEGA library (Java Engine for Genetic Algorithms). Full details on FORMA can be found in [48], which also reports examples of application to a supersonic blade profile (even though for axial Mach number < 1). For the present study, the original geometry parametrization was extended by including the possibility of optimizing the shape of the endwalls, still resorting to B-splines.

3 RESULTS AND DISCUSSION

3.1 Influence of endwall losses on turbine design

Boundary layers on hub and shroud walls are a relevant source of loss in supersonic turbines because of the huge velocity gradients in wall-normal direction: as shown in Eq. 2, dissipation is proportional to the cube of the free-stream velocity and since the flow is supersonic, the velocities are extremely high. Then the wetted surface is also larger because these turbines have usually a low-aspect ratio, which is the consequence of dimensionless ratios (chord/pitch and pitch/thickness) optimized to achieve the maximum efficiency.

Endwall boundary layers also play a role in reducing the available design space, by shifting the self-starting limit of the channel; this negative effect comes from the combination of two factors:

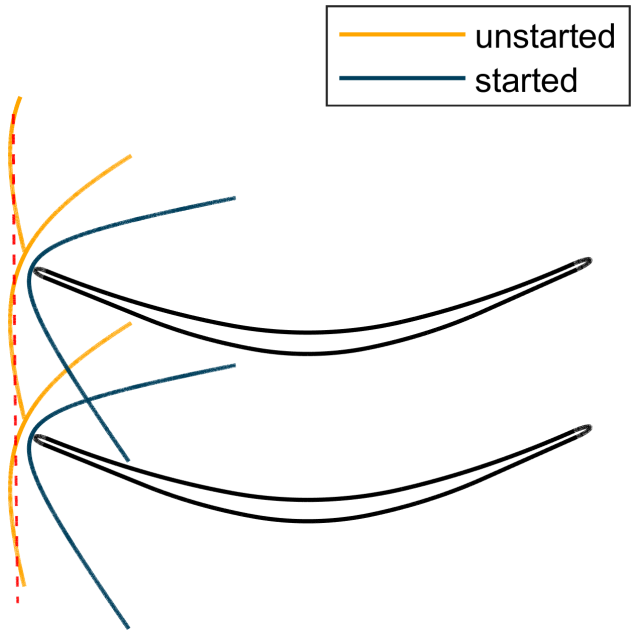

Fig. 5: THE DARK LINES DISPLAY THE SHOCK STRUCTURE ASSOCIATED TO A STARTED ROTOR OPERATING MODE, WHILE THE BRIGHT ONES SCHEMATIZE THE UNSTABLE BOW-SHOCK WAVE INTERSECTION IN FRONT OF THE LEADING EDGE THAT LEADS TO A NORMAL SHOCK WAVE AND ROTOR UNSTARTING.

i) A higher loss production lowers the stator outlet total pressure and the stator outlet Mach number by mass conservation.

ii) The growth of the endwall boundary layers progressively restricts the available area, due to the increase in their displacement thickness; converging channels behave like diffusing channel in supersonic flows and therefore the Mach numbers are further reduced.

A stator outlet Mach number lower than expected can be extremely critical because, as shown in Fig. 1, this can lead to a possible unstarting of the rotor blade row. This suggests that the endwall boundary layer and related loss must be taken properly into account when designing supersonic turbines.

In our experience, there is actually another scenario that leads to rotor unstarting even if the theoretical self-starting condition by Kantrowitz [39] is satisfied. In a low reaction machine, the intersection of the bow-shock waves generates a Mach phenomenon [49], identified by its characteristic structure composed of two slip lines and a normal shock wave between the two triple points (Fig. 4). If the relative Mach number at rotor inlet gets lower and lower, the bow-

shock waves widen reaching a state in which the intersection is no more happening within the channel but in front of the leading edge (Fig. 5). In this situation, the bow-shock waves with the Mach phenomena are in an unstable position and naturally transform into a normal shock wave that moves upwards and leads to rotor unstarting. Since supersonic turbines exhibit their highest efficiency for low reaction design points, it is recommended to be aware of this critical scenario; hence, the in-house mean-line code here applied avoids this feature by analyzing the predicted shock structure.

Turbine inlet conditions, presented in Tab. 1, were selected considering typical quantities for RDEs and high-pressure turbines [6, 13, 18, 22, 23, 50–52]. Then, parametric analyses based on the reaction degree X and peripheral velocity U were performed to find the optimal design point condition. The 240-points design space is characterized by 12 equally spaced points for U from 260 m/s to 500 m/s and 20 equally spaced points for X from 0 to 0.55; for each point, optimal solidity condition was searched by multiple runs of the mean-line thanks to its good agreement with CFD. Figures 6 and 7 present the results of these analyses as Smith diagrams through the flow and the stage loading coefficients. By inspecting the contours, it is immediately noticeable that these turbines behave differently than conventional subsonic turbines, which exhibit the highest efficiency at low flow and stage loading coefficients [53]. Conversely, efficient supersonic turbines are obtained for low flow coefficients but high stage loading coefficients (low reaction machine), because in those conditions the turbine extracts a large amount of work with reduced entropy production thanks to a lower relative Mach number at rotor inlet. In general terms, this outcome is not surprising, as the dominant loss mechanisms for supersonic turbines are notably different than those considered in historical turbomachinery studies. A further difference with respect to classical configurations is the self-starting condition that limits the design space. An in-depth description of this aspect can be found in paper [25].

The comparison between figures 6a and 6b confirms the importance of accounting for endwall losses in the preliminary analysis: as, expected, there is a significant drop in total-to-total efficiency for each design point, but the most critical variation is the shifting of the starting limit towards low load coefficient / high flow coefficient, that actually eliminated the most efficient configurations from

Table 1: INPUT PARAMETERS FOR THE REFERENCE DESIGN STAGE.

Mass flow rate [kg/s]	100
Inlet Mach number	2
Total Pressure [bar]	15
Inlet Axial Speed [m/s]	1445.46
Static Temperature [K]	1300

Table 2: BREAKDOWN OF STATOR AND ROTOR LOSSES AS PREDICTED BY THE MEAN-LINE CODE FOR THE TURBINE IN OPTIMAL LOADING CONDITION.

	Stator	**Rotor**
Shock losses [J/(kg K)]	25.46	8.68
Boundary and mixing losses [J/(kg K)]	14.00	8.86
Endwall losses [J/(kg K)]	21.72	11.70
Total losses [J/(kg K)]	61.18	29.24

the acceptable range.

To extend the available design space towards higher efficiency points, a variable stator blade height is a valuable option because the reduction in area caused by larger flow angles (high stage loading coefficient) is balanced by an increase in blade height at outlet section. Finally, the baseline configuration selected for all the subsequent optimization procedures is shown as point A in Fig. 7 with a stator blade height ratio of 1.2. A higher blade height ratio was not selected because stator outlet axial Mach number reduces with larger flow angles, making the machine more vulnerable to the unique incidence problem in off-design.

Since no loading criterium exists for these unconventional turbines, a novel automated optimization process based on Python, MATLAB and Ansys was developed to find the optimal loading value that minimizes the losses while delivering a sufficiently uniform flow at outlet, presented in paper [25]. To account for endwall losses also in this phase, the initial code, originally devised only for blade-to-blade simulations, was extended to perform 3D simulations. Figure 8 displays the results of the optimization process with a clear minimum for both stator and rotor.

In conclusion Tab. 2 contains a breakdown of stator and rotor losses in optimal loading condition; figure 9 gives an overview of the supersonic turbine and Tab. 3 collects the geometrical quantities for the blade definition.

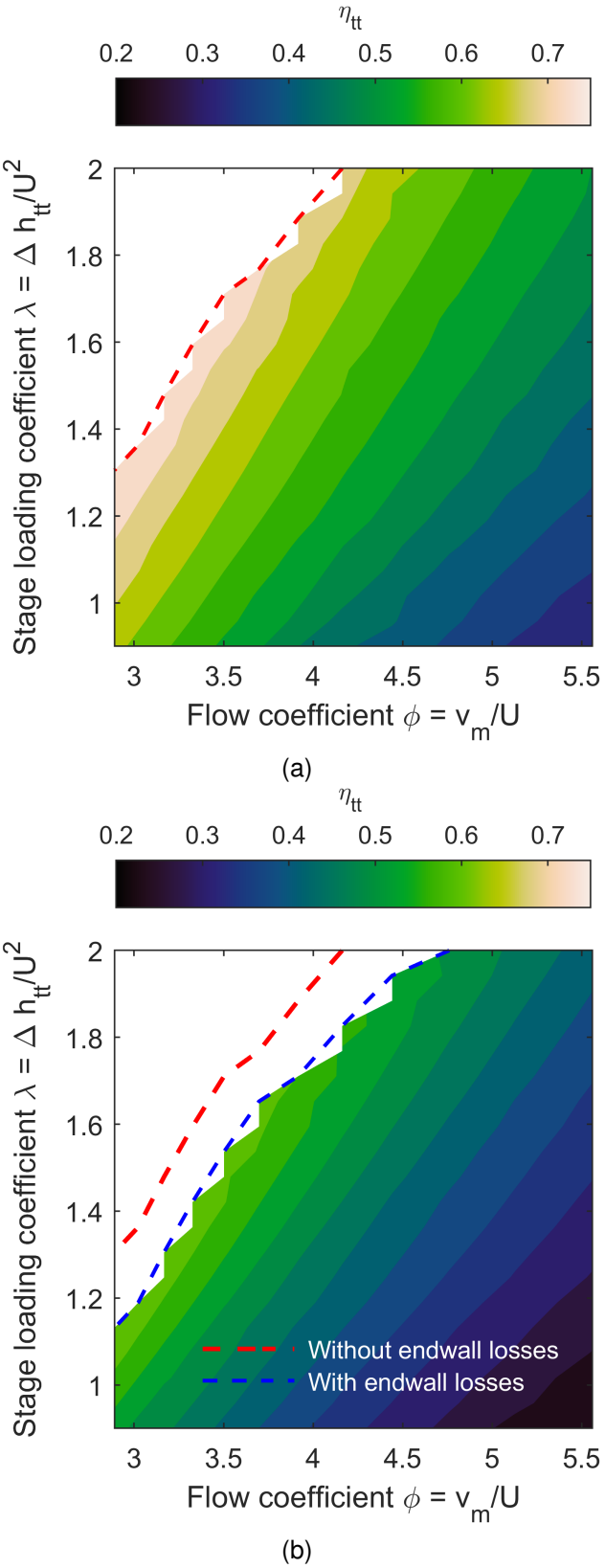

Fig. 6: STAGE TOTAL-TO-TOTAL EFFICIENCY FOR A STATOR BLADE HEIGHT RATIO OF 1 WITHOUT ENDWALL LOSSES (A) AND WITH ENDWALL LOSSES (B). THE RED AND BLUE DASHED LINES REPRESENT THE SELF-STARTING LIMIT.

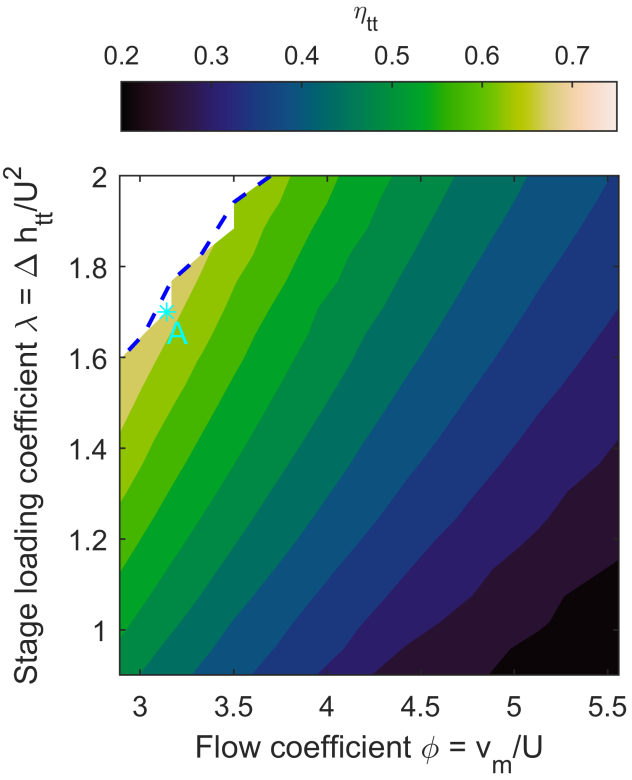

Fig. 7: STAGE TOTAL-TO-TOTAL EFFICIENCY FOR A STATOR BLADE HEIGHT RATIO OF 1.2 WITH ENDWALL LOSSES. THE BLUE DASHED LINE REPRESENTS THE SELF-STARTING LIMIT, WHILE POINT A IS THE DESIGN POINT SELECTED FOR THE OPTIMIZATION PROCEDURES.

Table 3: GEOMETRICAL DEFINITION OF THE TURBINE.

r_{1i}	345.0 mm	Chord	200 mm
H_1	57.35 mm	Peripheral velocity U_3	460 m/s
H_2	68.82 mm	Reaction degree X	0.15
H_3	68.82 mm	Stator blades	47
H_4	82.05 mm	Rotor blades	37

3.2 Turbine performance enhancement

In the previous section, a variable blade span configuration was selected for both the stator and the rotor, to shift the starting limit towards higher efficiencies. The simplest meridional configuration consists of a constant hub radius, while the shroud is linearly varied to obtain the desired inlet to outlet blade height ratio as represented in Fig. 9. Since the flow is supersonic, any sharp inward or outward bending of the endwall generates respectively a shock wave or an expansion wave; this

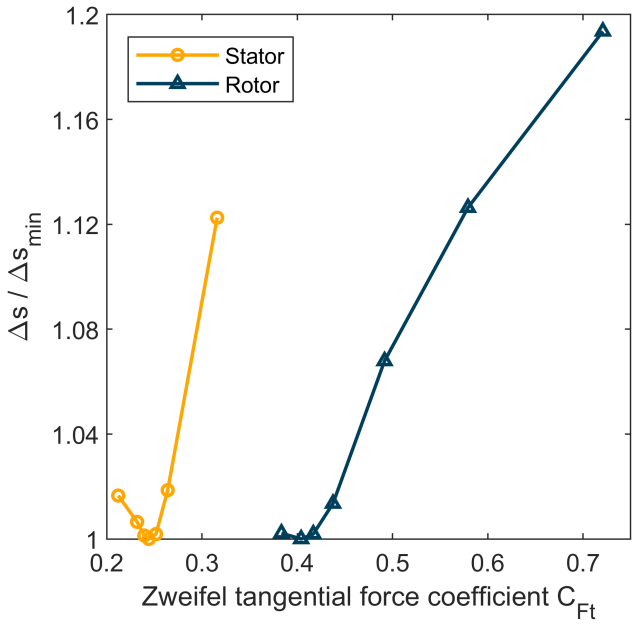

Fig. 8: ENTROPY GENERATED BY THE STATOR AND THE ROTOR AT DIFFERENT VALUES OF C_{Ft} TESTED IN THE OPTIMIZATION PROCEDURE.

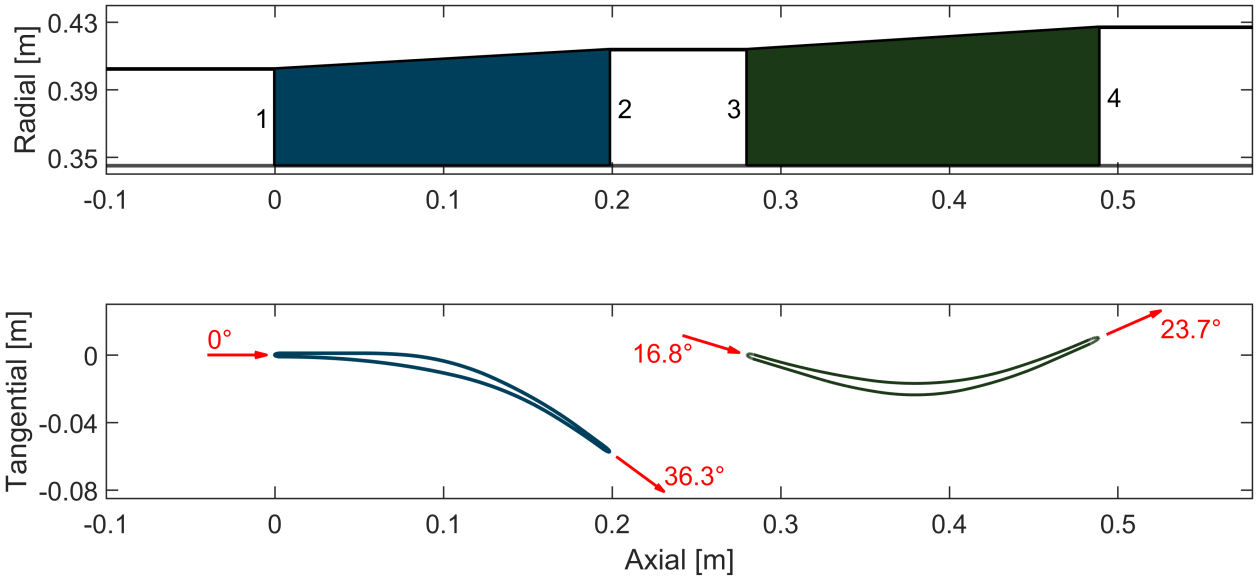

Fig. 9: OVERVIEW OF THE TURBINE GEOMETRY SELECTED FOR THE OPTIMIZATION PROCEDURES.

complication is clearly displayed by the meridional pressure distribution of the turbine, reported in Fig. 10, and the effect is not local, because the shocks and expansion waves are then reflected from hub to shroud along the entire channel.

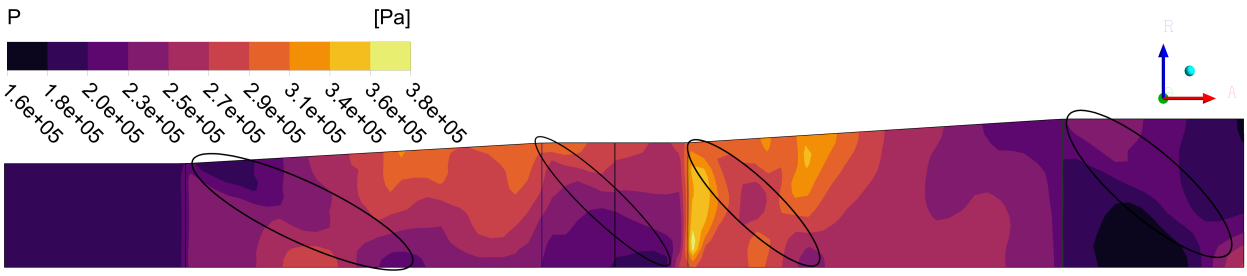

Fig. 10: CIRCUMFERENTIALLY AVERAGED PRESSURE CONTOURS ON THE MERIDIONAL PLANE. THE CIRCLED AREAS SURROUND THE FLOW AFFECTED BY THE EXPANSION AND SHOCK WAVES GENERATED BY THE ENDWALLS.

This issue can be solved by designing endwalls without corners but finding the optimal shape that minimizes losses is not trivial and a simple fillet of the endwall may lead to a suboptimal design. Hence, and in absence of robust criteria for supersonic endwall contouring in literature, the optimal shape of the endwall curves was searched in a systematic way by performing a CFD-based shape optimization using FORMA. Even though the geometry parametrization available in FORMA allows for a simultaneous optimization of the blade and of the endwalls, the present study is focused on the endwall design and hence the blade profiles were kept fixed throughout the optimization process.

The stator and rotor optimizations were performed separately to reduce computational cost and this strategy is allowable only for supersonic flows. Moreover, a 1.4 million cells mesh was adopted within the optimization as it represented the best compromise between accuracy and computational cost (20 minutes for each CFD run on a 40-core intel Xeon Gold 6242R CPU, for a total of 60 hours for the stator and 44 hours for the rotor). Then, all the assessments and comparisons of the optimal geometry with the baseline were based on stage simulations performed on the 9 million grid-independent mesh.

Different parametrizations, design spaces, objective functions, and constraints were tested. The outcome of this effort will be presented in the next paragraphs in the same order in which the turbine was optimized: at first the stator endwall shape optimization is reported; then a novel technique, tailored for supersonic inlet conditions, was employed for the three-dimensional redesign of the rotor; finally, the rotor endwall shape optimization was carried out.

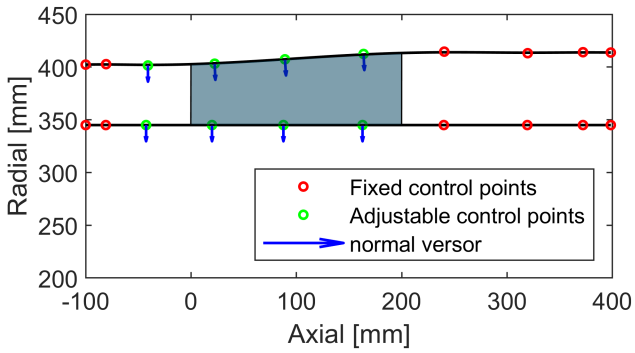

Fig. 11: B-SPLINE PARAMETRIZATION OF THE STATOR HUB AND SHROUD CURVES.

3.2.1 Stator endwall shape optimization

A proper interpolation of the curves is a key feature in the optimization process. 10 control points were used for the geometrical interpolation of both hub and shroud (Fig. 11); the adjustable control points are 4 and they are positioned so that the movable portion of the endwalls exceeds the length of the blade, from 2/5 of chord ahead of the leading edge to 1/5 of chord downstream the trailing edge (stator-rotor gap is 2/5 of chord). Stator inlet and outlet channel heights are fixed by the control points to maintain the constant area ratio given by the mean-line code, while the adjustable control points (ACP) move along the normal direction.

The maximum displacement of the ACP is 8 mm outwards and 4 mm inwards: this latter was determined analytically to have at least 10% margin from the self-starting limit because the inner variations reduce the cross-sectional area. The 10% safety margin might seem small, but it is relevant to remember that the limit for the unstarting of an already started channel is much lower (Fig. 1).

The objective function is the minimization of the entropy generated by the blade row, which is measured within the optimization as the difference between the related mass-flow averaged values on the inlet and outlet sections. The discrepancy between the mixed-out entropy and the mass-flow average one is overcome by placing downstream an additional volume, which is bounded by free slip walls, to gradually mix the flow and dampen all non-uniformities (Fig. 11). Theoretically, an infinitely long distance is required to reach the mixed-out state, but at one chord distance, it

was observed that the difference between the mass-flow average entropy value and the mixed out one is below 1%.

The baseline stator outlet flow angle is characterized by an under-turning of 1.51° compared to the value prescribed by the mean-line code; this under-turning results from the flow deviation induced by the last shock wave reflection in the unguided-turning region and by the complex pattern of shocks and expansion fans established at the trailing edge. Different models were implemented and tried in the mean-line code, but none of them gave a satisfactory prediction of the deviation angle. Maksiuta in [54] claimed that the meridional shape of the turbine flow path affects the deviation angle and following this concept, the meridional shape can be modified to reduce the deviation angle. Therefore, a constraint was also introduced in the optimization process to force the stator outlet flow angle to be within 1 degree from the mean-line code value.

This concept is confirmed by Fig. 12, which displays an overview of the performance of all the geometries tested during the optimization process, while Fig. 13 compares the final optimal meridional shape with the baseline one. In the optimal shape, the hub and shroud curves start to converge before the leading edge to reduce the Mach number seen by the leading edge; this is very beneficial because a major source of loss in a supersonic turbine is the leading-edge bow shock and this optimal configuration allows a significant reduction of the shock-related dissipation. Then the curves smoothly open to maintain the inlet to outlet channel height ratio.

The stator blade with optimal endwall curves produces an entropy increase (mixed-out) of 57.86 J/(kg K), which is 6.49% lower than the baseline; the deviation angle was successfully lowered from 1.51° to 0.94° and the stage total-to-total efficiency reached 67.97%, which is a 1.92% higher than the baseline.

3.2.2 Rotor three-dimensional blade design

The original rotor profile was generated by the MOC with the Mach number and flow angle predicted by the mean-line code. To improve the geometry and minimize incidence losses, the first step is to consider the true Mach number and flow angle delivered by the stator, but both quantities manifest a clear dependence on the radial location; therefore, it was conceived the idea

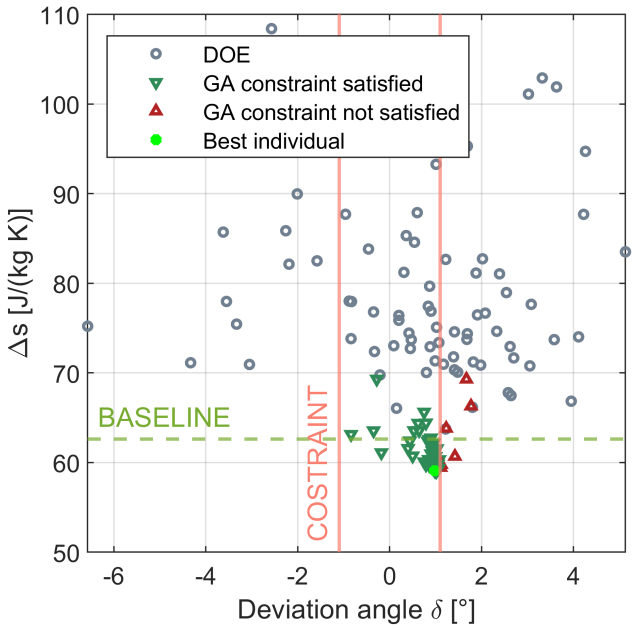

Fig. 12: DEVIATION ANGLE AND ENTROPY PRODUCTION OF ALL THE GEOMETRIES TESTED IN THE STATOR OPTIMIZATION PROCESS.

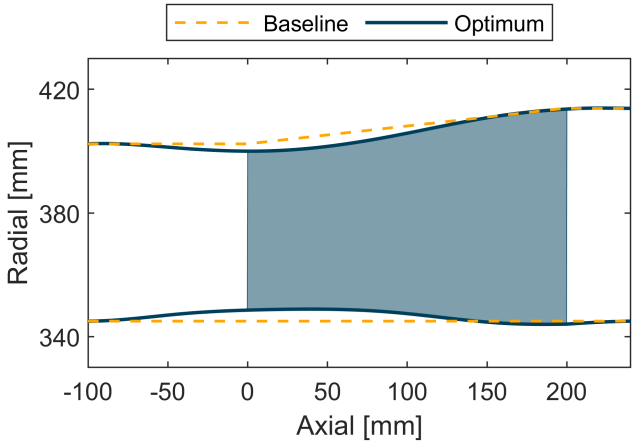

Fig. 13: COMPARISON BETWEEN THE STATOR BASELINE MERIDIONAL SHAPE AND THE OPTIMAL ONE.

to build the rotor blade by interpolating the profiles generated by the MOC at different heights.

As demonstrated by Fig. 7, in supersonic turbines the designer can maximize both efficiency and work without a compromise; hence, to improve efficiency and generate more power, the relative rotor outlet angle can be further increased from 23.7° to 35° to reach the 10% safety margin from the starting limit, overtaking the original value proposed by the mean-line code to obtain a

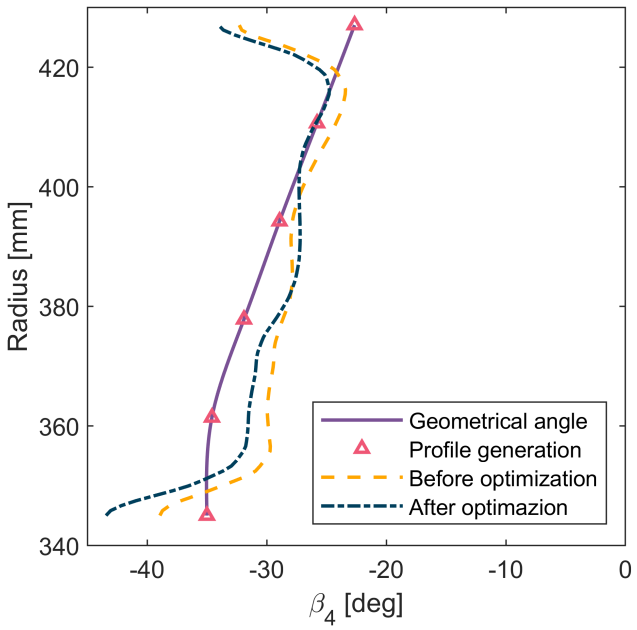

Fig. 14: THE SOLID LINE IS THE GEOMETRICAL ANGLE PRESCRIBED AT ROTOR OUTLET FOR THE 3D DESIGN, WHILE THE TRIANGLES REPRESENT THE LOCATION WHERE THE PROFILES WERE GENERATED TO BUILD THE BLADE. THE DASHED AND THE DASHED-DOTTED LINE ARE RESPECTIVELY THE FLOW ANGLE EXTRACTED AT 1/5 OF CHORD FROM THE TRAILING EDGE BEFORE AND AFTER ROTOR ENDWALL OPTIMIZATION.

purely axial rotor outlet flow (please consider that this is not the last stage that requires kinetic energy minimization). However, in a two-dimensional MOC the inlet and outlet Mach numbers and the inlet and outlet flow angles are linked by the 2D continuity equation; thus, at higher radius where the inlet Mach number is lower, the outlet angle was reduced because the 2D MOC does not consider the increase in Mach number due to an increase in cross-sectional area. The trend of the relative outlet angle is shown in Fig. 14 with a radially averaged value of 30.1 °, while a view of the 3D rotor blade geometry is displayed in Fig. 15.

Total-to-total efficiency and power extracted by the turbine are 69.85% and 37.42 MW, which are respectively 4.74% and 9.10% higher than the baseline. The entropy generated by the rotor increased from 34.7 J/(kg K) to 37.1 J/(kg K), which is reasonable due to the increase in rotor outlet flow angle. Considering these results, the concept of a three-dimensional rotor blade design tailored on the flow delivered by the stator was beneficial in further enhancing the turbine performance.

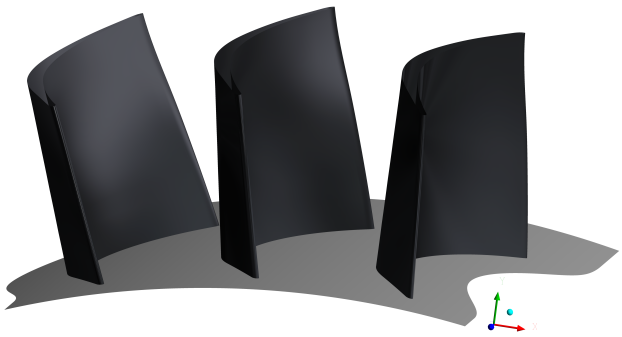

Fig. 15: VIEW OF THE THREE-DIMENSIONAL ROTOR BLADE.

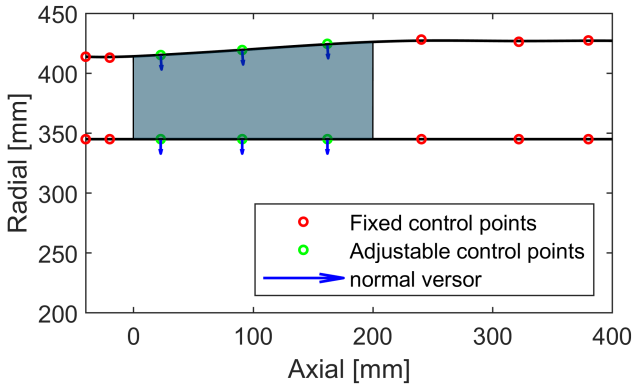

Fig. 16: B-SPLINE PARAMETRIZATION OF THE ROTOR HUB AND SHROUD CURVES.

3.2.3 Rotor endwall shape optimization

The interpolation of the rotor hub and shroud curves was made by selecting 8 control points with 3 of them adjustable as shown in Fig. 16. Rotor inlet to outlet channel height ratio was kept fixed to the value prescribed by the mean-line code and the ACP were positioned to modify the endwalls from 1/10 of chord upstream the leading edge to 1/5 of chord downstream the trailing edge. Considering a 10% safety margin from the starting limit, the inward displacement is restricted to 1 mm for the first ACP and 4 mm for the other two; the outward displacement for all the ACP is 5 mm. The objective function is the minimization of the entropy produced by the rotor blade, while the outlet flow angle was constrained to be within 0.5° from the geometrical angle, calculated as the integral average in radial direction.

Figure 17 presents a comparison between the optimal profile and the baseline one. As seen for

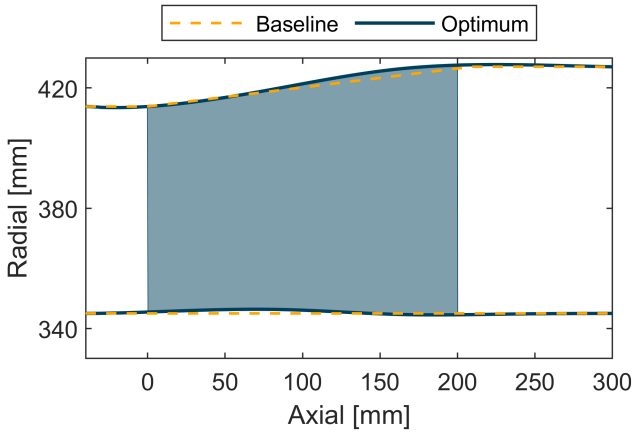

Fig. 17: COMPARISON BETWEEN THE ROTOR BASELINE MERIDIONAL SHAPE AND THE OPTIMAL ONE.

Table 4: DETAILED QUANTITATIVE COMPARISON BETWEEN THE RESULTS OF THE FOUR CONSECUTIVE DESIGN STEPS.

	Mean-line code	**Optimal Loading**	**Stator Endwall optimization**	**Rotor 3D blade design**	**Rotor Endwall Optimization**	**(Final-Initial)/(Initial)**
η_{tt}	67.73 %	66.69 %	67.97 %	69.85 %	70.60 %	+5.86 %
Power [MW]	35.97	34.30	34.79	37.42	38.30	+11.67 %
Δs_{stator} [J/(kg K)]	61.18	61.88	57.86	57.89	58.09	-6.12 %
Δs_{rotor} [J/(kg K)]	29.24	34.40	34.69	37.12	35.56	+3.35 %
M_2	1.69	1.71	1.73	1.73	1.73	
M_{4W}	1.52	1.49	1.49	1.44	1.40	
α_2 [deg]	36.28	34.77	35.34	35.35	35.39	
β_4 [deg]	-23.71	-24.32	-24.13	-28.34	-30.26	

the stator, also rotor hub and shroud curves initially converge to moderate the leading-edge shock losses, but in this case the reduction in cross-sectional area reduction is significantly restricted by the closer starting limit. Then the curves diverge, and especially the shroud expands rapidly and reaches the final height before the trailing edge.

The optimal meridional shape improves considerably the flow guiding and as shown in Fig. 14, rotor outlet flow angle is closer to the geometrical angle in almost all radial positions. The deviation angle, determined as the difference between the mass-flow average outlet flow angle and the radially averaged geometrical angle, decreased from the 1.71° of the 3D rotor without

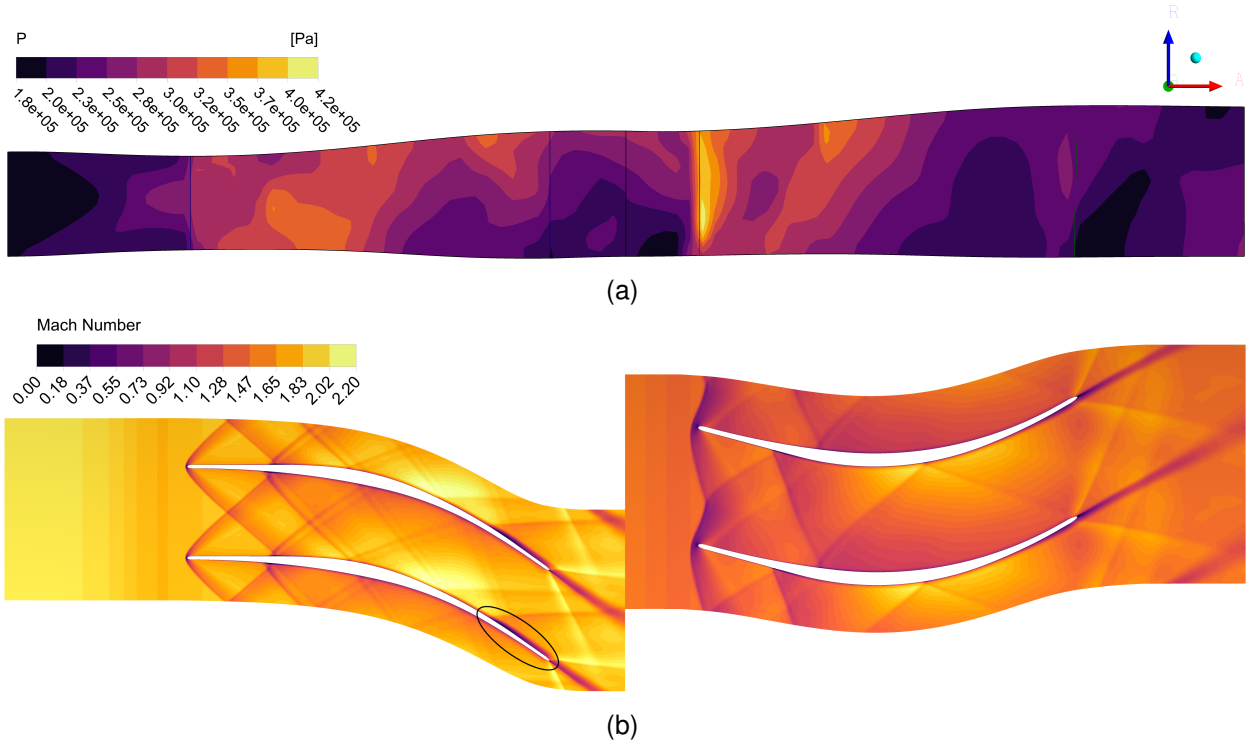

Fig. 18: FLOW FIELD VISUALIZATION OF THE FINAL OPTIMIZED TURBINE: AVERAGED PRESSURE CONTOURS ON THE MERIDIONAL PLANE (A) AND MACH CONTOURS ON THE BLADE-TO-BLADE PLANE AT MIDSPAN(B). THE CIRCLED AREA HIGHLIGHTS A SLIGHT SEPARATION ON STATOR SUCTION SIDE.

optimal endwalls to 0.19°.

The entropy generated by the rotor optimal meridional shape is 35.56 J/(kg K) (-4.22% from the previous geometry). Considering the contributions of all the three steps of the endwall contouring design, the total-to-total efficiency of the stage rises to 70.6%, i.e. an increase of 5.86% with respect to the baseline design with streamwise-linear endwall. The improvement gained for the rotor was lower than the stator one because for the rotor the Kantrowitz starting limit was closer and therefore the optimization was more constrained.

A complete overview of the final optimized turbine flow field is displayed by the meridional and blade-to-blade planes (fig. 18). The converging channel reduces the stator inlet Mach number and then the shock losses; The included angle between the bow shock branches widens increasing the number of shock reflections in the channel. On the suction side, the last oblique shock reflection

produces a slight separation. In the rotor, a Mach phenomenon is generated by the intersection of the bow-shock waves, but overall compared to the stator the shocks are weaker and the flow is more uniform. The pressure contours on the meridional plane suggest an improved pressure distribution and uniformity, while the expansion fans and shock waves observed in Figure 10 and generated by the corners in the baseline shroud curve have disappeared.

In conclusion, Table 4 reports all the relevant data to retrace the evolution of the turbine performance: stator and rotor optimal loading condition, stator endwall optimization, rotor three-dimensional blade design and rotor endwall optimization.

3.2.4 Off-design analysis

Turbine optimization was carried out considering design flow conditions at inlet, but the optimum turbine has still to prove superior performance also in off-design. The turbine inlet Mach number and inlet flow angle are selected for the off-design analysis because the flow released by the rotating detonation combustion chamber is characterized by large fluctuations on these variables [24].

The range of Mach number considered is 2-2.6, while lower values than the design one were not simulated. To reliably simulate lower Mach numbers, unsteady calculations, which include the transient from the self-started design condition, are required to properly simulate not self-started inlet conditions as also depicted in Fig. 1. In the present analysis static quantities were maintained constant, while total ones increase as observed in the trends reported in [24].

At limited overspeed, the optimized turbine performs better than the baseline with a higher total-to-total efficiency and higher work extraction (Fig. 19a); at very high Mach numbers, the rotors of both turbines are characterized by large flow separation which leads to a rapid decrease in efficiency. Stator meridional shape optimization reduces entropy production at all Mach numbers (Fig. 19b); however, rotor losses for the optimum configuration are significantly higher than the baseline one and the rotor three-dimensional design is accountable for this for two reasons: 1) the rotor outlet flow angle was increased of 6°, which enhances and anticipates boundary layer separation on rotor suction side; 2) rotor inlet design was tailored on the flow delivered by the

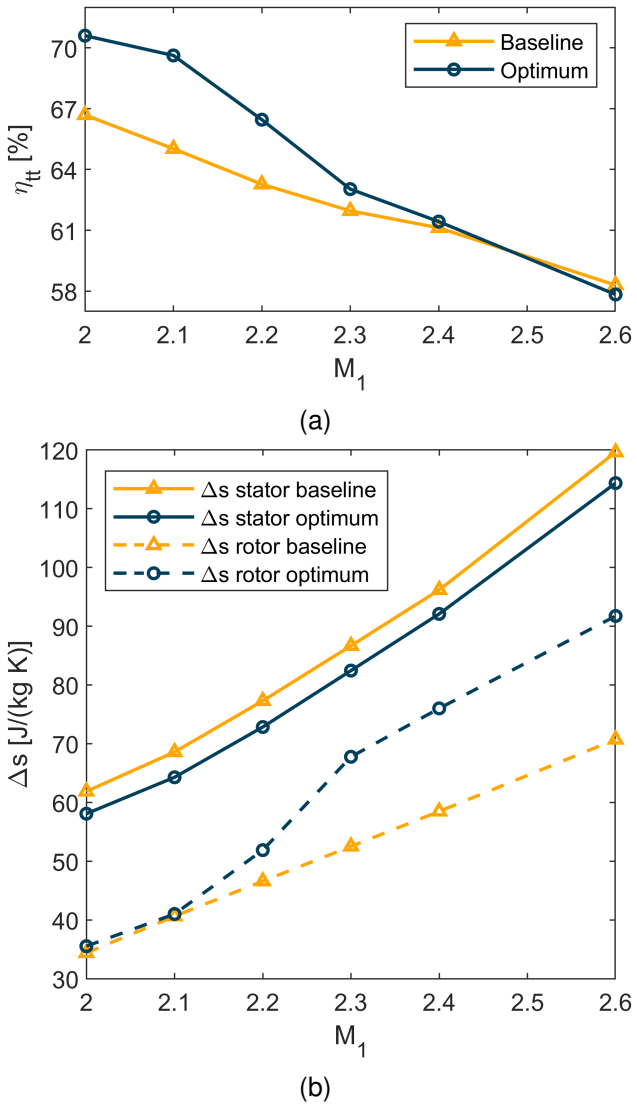

Fig. 19: COMPARISON OF TOTAL-TO-TOTAL EFFICIENCY (A) AND STATOR AND ROTOR ENTROPY PRODUCTION (B) BETWEEN THE BASELINE AND THE OPTIMIZED TURBINE AT VARIOUS INLET MACH NUMBERS.

stator in design condition, which is considerably different from the flow released at extremely high inlet Mach numbers.

For the angle off-design analysis, the incidence angle was varied from -9° to 9°, while the Mach number and all the other quantities were maintained constant. Higher inlet flow angles were not considered because the large flow separation on the suction side for positive angles and on the pressure side for negative angles led to oscillatory behavior in the residuals and the criteria

for convergence given in section 2.1 were not achieved; these inlet conditions require unsteady calculations to properly capture the unsteady flow features.

The off-design simulations were performed only on the stator since it is the most affected by inlet angle fluctuations; figure 20a displays the excellent flow guiding capabilities of the stator as the $\pm 9°$ perturbations at inlet are reduced below $\pm 1°$ at the outlet and therefore the rotor performance is only marginally influenced by the stator inlet angle. This demonstrates the necessity of the stator in the architecture of a supersonic turbine as it reduces the large fluctuations given by the detonation combustor and attenuates by 90% the high frequency perturbations [55], which can be critical for the endurance of the rotor blades and for possible resonance phenomena. It is also interesting to observe that the baseline geometry and the optimum one have an opposite deviation angle trend, with under-turning and over-turning mirrored respect to the design angle. The onset of under-turning or over-turning is strictly dependent on the shock pattern at stator trailing edge whose features are deeply interconnected with the endwall geometry.

The robustness of the meridional shape optimization to inlet flow angle fluctuations is excellent (Fig. 20b): the optimized blade not only generates less entropy than the baseline at all incidence angles, but the decrease in performance of the baseline is also faster; hence, endwall optimization led to a geometry that prevails over the baseline in design and in off-design. For both geometries, the increase in losses is steeper at negative incidence angles compared to the positive ones: this can be explained by the fact that a separation of the flow on the suction side (positive incidence angles) reattaches more easily thanks to an accelerating flow and a negative pressure gradient. Notice also that the optimized blade generates less entropy at -3° compared to the design condition, because the slight flow separation observed on the suction side in design condition vanishes (Fig. 18).

In conclusion, meridional shape optimization for supersonic turbines proved to be a robust procedure to Mach number and inlet flow angle fluctuations since the concept of reducing shock losses and deviation angles is valid in design as well as in off-design. Rotor three-dimensional design behaves well at limited overspeed but suffers when the off-design conditions are far from the design ones.

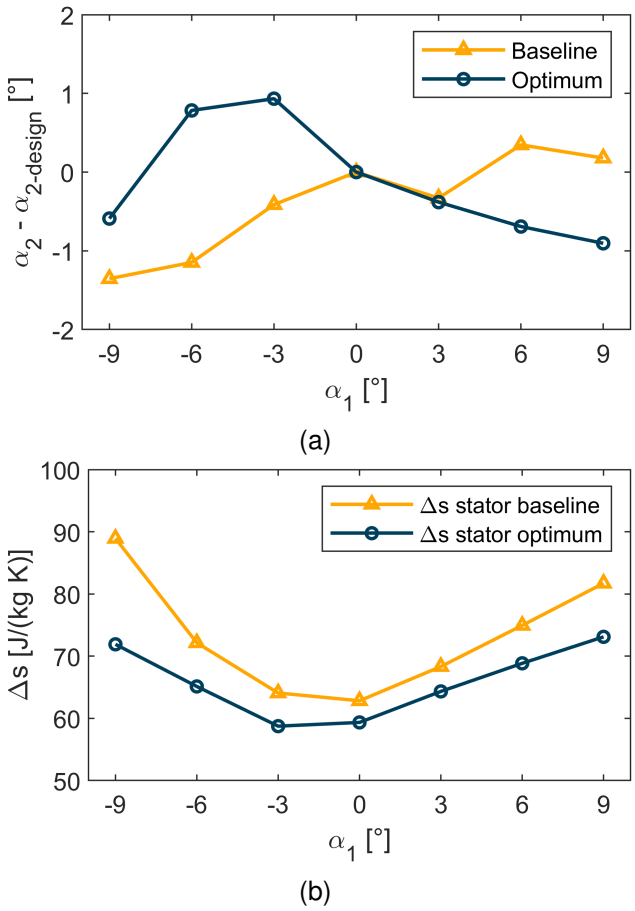

Fig. 20: COMPARISON BETWEEN THE BASELINE AND THE OPTIMIZED TURBINE FOR THE STATOR OUTLET FLOW ANGLE (A) AND FOR THE STATOR ENTROPY PRODUCTION (B) AT VARIOUS STATOR INLET FLOW ANGLES.

4 CONCLUSIONS

This paper presents and discusses the importance of endwalls in the design of a supersonic stage for RDE applications. It was observed that endwall losses are a major contributor ($\approx$ 30%) in the overall loss breakdown, because of the considerable dissipation generated by the huge velocity gradients in the endwall surface boundary layers. The progressive growth of the boundary layer also decreases the outlet Mach number in a supersonic flow. The outcome is a shifting of the starting limit which eliminates the configurations with the highest efficiencies.

Parametric analyses reveal that a variable blade height mitigates the starting limit and makes available the inaccessible more performing design points, but the baseline meridional shape with streamwise-linear endwall is inadequate because the corners produce systems of compression

and expansion waves that have detrimental effects on the efficiency.

The paper presents a design methodology with a sequence of four consecutive procedures: 1) stator and rotor optimal loading condition was found by an automated CFD-based optimization process; 2) stator meridional shape was optimized by FORMA, which resorts to surrogate evolutionary strategies; 3) rotor three-dimensional geometry was redesigned with a novel technique based on the MOC and tailored on the flow delivered by the stator; 4) rotor endwalls were optimized by FORMA. Thanks to this procedure, the optimized turbine is 6% more efficient and produces 12% more power than the baseline turbine. Endwall optimization carries two additional benefits: a more precise flow guiding at the outlet of each cascade and an improved pressure distribution and uniformity. Both these advantages improve the stage efficiency and facilitate the design of the following stages.

Finally, endwall shape optimization proved to be robust in tolerating off design conditions, thus improving the efficiency over a wider range of operation.

NOMENCLATURE

a	Ellypse semi-major axis [m]
A	Area [m^2]
b	Ellypse semi-minor axis [m]
c	Chord [m]
C_d	Dissipation coefficient [-]
C_{ft}	Zweifel's tangential force coefficient [-]
g	Blade pitch [m]
H	Blade height [m]
M	Mach number [-]
p	Pressure [Pa]
r	Radius [m]
Re_θ	Momentum thickness Reynolds number [-]
s	Specific entropy [$Jkg^{-1}K^{-1}$]

T Temperature [K]

U Peripheral velocity [m/s]

v Velocity [m/s]

X Stage reaction: static rotor enthalpy variation/Euler work [-]

α Absolute flow angle with respect to axial direction [°]

β Relative flow angle with respect to axial direction [°]

θ Momentum thickness [m]

η_{tt} Total-to-total efficiency: Euler work/total to total isentropic head [-]

λ Stage loading coefficient [-]

ξ Entropy loss coefficient [-]

ρ Density [kgm^{-3}]

ϕ Flow coefficient [-]

Subscripts

1,2 Stator inlet and outlet, respectively

3,4 Rotor inlet and outlet, respectively

ew Endwall

i Inner

in Inlet

m Meridional

o Outlet

th Throat

W Relative frame of reference

Acronyms

ACP Adjustable Control Points

CFD Computational Fluid Dynamics

MOC Method of Characteristics

RDE Rotating Detonation Engine

REFERENCES

[1] Brouckaert JF., 2019, "An Outlook on the Future of Turbofans and Aircraft Propulsion Systems," In EASN Conference.

[2] Gabrielli, P., Gazzani, M., Martelli, E., and Mazzotti, M., 2018, "Optimal design of multi-energy systems with seasonal storage," *Applied Energy*.

[3] Wintenberger, E., and Shepherd, J. E., 2006, "Thermodynamic Cycle Analysis for Propagating Detonations," *Journal of Propulsion and Power,* **22**(3), may, pp. 694–698.

[4] Jones, S. M., and Paxson, D. E., 2013, "Potential Benefits to Commercial Propulsion Systems from Pressure Gain Combustion," In *49th AIAA/ASME/SAE/ASEE Joint Propulsion Conference*, Joint Propulsion Conferences. American Institute of Aeronautics and Astronautics, jul.

[5] Frolov, S. M., Dubrovskii, A. V., and Ivanov, V. S., 2013, "Three-dimensional numerical simulation of operation process in rotating detonation engine," *Progress in Propulsion Physics,* **4**, pp. 467–488.

[6] Sousa, J., Paniagua, G., and Collado Morata, E., 2017, "Thermodynamic analysis of a gas turbine engine with a rotating detonation combustor," *Applied Energy,* **195**, pp. 247–256.

[7] Strakey, P., Ferguson, D., Sisler, A., and Nix, A., 2016, "Computationally Quantifying Loss Mechanisms in a Rotating Detonation Engine," In *54th AIAA Aerospace Sciences Meeting*, AIAA SciTech Forum. American Institute of Aeronautics and Astronautics, jan.

[8] Claflin, S., Sonwane, S., Lynch, E., and Stout, J., 2014, "Recent advances in power cycles using rotating detonation engines with subcritical and supercritical CO2," In 4th International Symposium - Supercritical CO2 Power Cycles.

[9] Frolov, S. M., Aksenov, V. S., and Ivanov, V. S., 2015, "Experimental proof of Zel'dovich cycle efficiency gain over cycle with constant pressure combustion for hydrogen–oxygen fuel mixture," *International Journal of Hydrogen Energy,* **40**(21), pp. 6970–6975.

[10] Wolański, P., 2015, "Application of the Continuous Rotating Detonation to Gas Turbine," *Applied Mechanics and Materials,* **782**, pp. 3–12.

[11] Naples, A., Hoke, J., Battelle, R. T., Wagner, M., and Schauer, F. R., 2017, "RDE Implementation into an Open-Loop T63 Gas Turbine Engine," In *55th AIAA Aerospace Sciences Meeting*,

AIAA SciTech Forum. American Institute of Aeronautics and Astronautics, jan.

[12] Fotia, M. L., Schauer, F., Kaemming, T., and Hoke, J., 2015, "Experimental Study of the Performance of a Rotating Detonation Engine with Nozzle," *Journal of Propulsion and Power,* **32**(3), dec, pp. 674–681.

[13] Paxson, D. E., and Naples, A., 2017, "Numerical and analytical assessment of a coupled rotating detonation engine and turbine experiment," In AIAA SciTech Forum - 55th AIAA Aerospace Sciences Meeting.

[14] Bach, E., Bohon, M. D., Paschereit, C. O., and Stathopoulos, P., 2019, "Influence of nozzle guide vane orientation relative to RDC wave direction," In AIAA Propulsion and Energy Forum and Exposition, 2019.

[15] Bach, E., Bohon, M. D., Paschereit, C. O., and Stathopoulos, P., 2019, "Impact of outlet restriction on RDC performance and stagnation pressure rise," In AIAA Scitech 2019 Forum.

[16] Anand, V., and Gutmark, E., 2019, "Rotating detonation combustors and their similarities to rocket instabilities," *Progress in Energy and Combustion Science,* **73**, pp. 182–234.

[17] Ma, J. Z., Luan, M.-Y., Xia, Z.-J., Wang, J.-P., Zhang, S.-j., Yao, S.-b., and Wang, B., 2020, "Recent Progress, Development Trends, and Consideration of Continuous Detonation Engines," *AIAA Journal,* **58**(12), nov, pp. 4976–5035.

[18] Paniagua, G., Iorio, M. C., Vinha, N., and Sousa, J., 2014, "Design and analysis of pioneering high supersonic axial turbines," *International Journal of Mechanical Sciences,* **89**, pp. 65–77.

[19] Sousa, J., and Paniagua, G., 2015, "Entropy minimization design approach of supersonic internal passages," *Entropy*.

[20] Braun, J., Saavedra, J., and Paniagua, G., 2017, "Evaluation of the unsteadiness across nozzles downstream of rotating detonation combustors," *AIAA SciTech Forum - 55th AIAA Aerospace Sciences Meeting*(January), pp. 1–12.

[21] Sousa, J., Paniagua, G., and Saavedra, J., 2017, "Aerodynamic response of internal passages to pulsating inlet supersonic conditions," *Computers and Fluids,* **149**, pp. 31–40.

[22] Liu, Z., Braun, J., and Paniagua, G., 2019, "Characterization of a Supersonic Turbine Downstream of a Rotating Detonation Combustor," *Journal of Engineering for Gas Turbines and*

Power, **141**(3), pp. 1–13.

[23] Braun, J., Saracoglu, B. H., and Paniagua, G., 2017, "Unsteady performance of rotating detonation engines with different exhaust nozzles," *Journal of Propulsion and Power,* **33**(1), pp. 121–130.

[24] Braun, J., Paniagua, G., and Ferguson, D., 2021, "Aero-Thermal Characterization of Accelerating and Diffusing Passages Downstream of Rotating Detonation Combustors," In ASME Turbo Expo 2021, pp. GT2021–59111.

[25] Mushtaq, N., Colella, G., and Gaetani, P., 2022, "Design and Parametric Analysis of a Supersonic Turbine for Rotating Detonation Engine Applications," *International Journal of Turbomachinery, Propulsion and Power,* **7**(1).

[26] Liu, Z., Braun, J., and Paniagua, G., 2020, "Thermal power plant upgrade via a rotating detonation combustor and retrofitted turbine with optimized endwalls," *International Journal of Mechanical Sciences,* **188**, p. 105918.

[27] Bufi, E. A., and Cinnella, P., 2018, "Preliminary Design Method for Dense-Gas Supersonic Axial Turbine Stages," *Journal of Engineering for Gas Turbines and Power,* **140**(11), aug.

[28] Schlichting, H., and Gersten, K., 2000, *Boundary-Layer Theory*, 8th ed. Springer.

[29] Sharma, O. P., and Butler, T. L., 1987, "Predictions of Endwall Losses and Secondary Flows in Axial Flow Turbine Cascades," *Journal of Turbomachinery,* **109**(2), apr, pp. 229–236.

[30] Coull, J. D., 2017, "Endwall Loss in Turbine Cascades," *Journal of Turbomachinery,* **139**(8), mar.

[31] Persico, G., Pini, M., Dossena, V., and Gaetani, P., 2015, "Aerodynamics of Centrifugal Turbine Cascades," *Journal of Engineering for Gas Turbines and Power,* **137**(11), nov.

[32] Druguet, M. C., and Zeitoun, D. E., 2003, "Influence of numerical and viscous dissipation on shock wave reflections in supersonic steady flows," *Computers and Fluids*.

[33] Sod, G. A., 1977, "A numerical study of a converging cylindrical shock," *Journal of Fluid Mechanics*.

[34] Settles, G. S., and Dodson, L. J., 1991, "Hypersonic shock/boundary-layer interaction database," In AIAA 22nd Fluid Dynamics, Plasma Dynamics and Lasers Conference, 1991.

[35] Settles, G., and Dodson, L., 1994, "Hypersonic shock/boundary-layer interaction database: new and corrected data," *Pennsylvania State Univ. Report*.

[36] Settles, G. S., Fitzpatrick, T. J., and Bogdonoff, S. M., 1979, "Detailed study of attached and separated compression corner flowfields in high reynolds number supersonic flow," *AIAA Journal*.

[37] Celik, I. B., Ghia, U., Roache, P. J., Freitas, C. J., Coleman, H., and Raad, P. E., 2008, "Procedure for estimation and reporting of uncertainty due to discretization in CFD applications," *Journal of Fluids Engineering, Transactions of the ASME,* **130**(7), pp. 780011–780014.

[38] Prasad, A., 2004, "Calculation of the Mixed-Out State in Turbomachine Flows," *Journal of Turbomachinery,* **127**(3), mar, pp. 564–572.

[39] Kantrowitz, A., and Donaldson, C., 1945, "Preliminary inversitagtion of supersonic diffusers," *NACA Wartime reports*.

[40] Starken, H., Yongxing, Z., and Schreiber, H.-A., 1984, Mass Flow Limitation of Supersonic Blade Rows due to Leading Edge Blockage, jun.

[41] Goldman, L. J., and Vanco, M. R., 1971, "Computer Program for Design of Two-Dimensional Sharp-Edged-throat Supersonic Nozzle with Boundary-Layer Correction," *NASA*.

[42] Moeckel, 1921, "Approximate method for predicting form and location of detached shock waves ahead of plane or axially symmetric bodies," *NASA TN 1921,* **211**(1), p. 130.

[43] Anderson, J. D., 2003, *Modern Compressible Flow: With Historical Perspective* Aeronautical and Aerospace Engineering Series. McGraw-Hill Education.

[44] Stratford, B. S., and Beavers, G. S., 1961, "The Calculation of the Compressible Turbulent Boundary Layer in an Arbitrary Pressure Gradient - A Correlation of certain previous Methods," *Aeronautical Research Council Reports*(3207).

[45] Stewart, W., 1955, "Analysis of two-dimensional compressible-flow loss characterisitics downstream of turbomachine blade rows in terms of basic boundary-layer characteristics," *NACA Technical Note 3515*.

[46] Denton, J. D., 1993, "The 1993 IGTI Scholar Lecture: Loss Mechanisms in Turbomachines," *Journal of Turbomachinery,* **115**(4), oct, pp. 621–656.

[47] Moore, J., and Moore, J. G., 1983, Entropy Production Rates From Viscous Flow Calculations: Part I — A Turbulent Boundary Layer Flow, mar.

[48] Persico, G., Rodriguez-Fernandez, P., and Romei, A., 2019, "High-Fidelity Shape Optimization of Non-Conventional Turbomachinery by Surrogate Evolutionary Strategies," *Journal of Turbomachinery*.

[49] Délery, J., and Dussauge, J. P., 2009, "Some physical aspects of shock wave/boundary layer interactions," *Shock Waves*.

[50] Sun, C., Zheng, H., Li, Z., Zhao, N., Qi, L., and Guo, H., 2019, "Effects of diverging nozzle downstream on flow field parameters of rotating detonation combustor," *Applied Sciences (Switzerland),* **9**(20).

[51] Schwer, D., and Kailasanath, K., 2011, "Numerical Study of the Effects of Engine Size n Rotating Detonation Engines,".

[52] Rankin, B. A., Fotia, M. L., Naples, A. G., Stevens, C. A., Hoke, J. L., Kaemming, T. A., Theuerkauf, S. W., and Schauer, F. R., 2017, "Overview of performance, application, and analysis of rotating detonation engine technologies," *Journal of Propulsion and Power*.

[53] Smith, S. F., 1965, "A Simple Correlation of Turbine Efficiency," *The Journal of the Royal Aeronautical Society,* **69**(655), pp. 467–470.

[54] Maksiuta, D., Moroz, L., Burlaka, M., and Pastrikakis, V., 2019, "Deviation Angle in a Turbine Nozzle Cascade with Convergent Meridional Shape of Flow Path," In 5th International Seminar on ORC Power Systems.

[55] Sousa, J., Paniagua, G., and Saavedra, J., 2017, "Aerodynamic response of internal passages to pulsating inlet supersonic conditions," *Computers and Fluids*.

LIST OF FIGURES

LIST OF TABLES